




Physical origin of relativistic plasmons in a two-dimensional electron system

V. M. Muravev,¹ P. A. Gusikhin ¹, A. M. Zarezin ^{1,2}, A. A. Zabolotnykh,³ V. A. Volkov,³ and I. V. Kukushkin ¹

¹*Institute of Solid State Physics, RAS, Chernogolovka, 142432 Russia*

²*Moscow Institute of Physics and Technology, Dolgoprudny, 141700 Russia*

³*Kotelnikov Institute of Radio-engineering and Electronics of the RAS, Mokhovaya 11-7, Moscow 125009, Russia*



(Received 19 April 2020; revised 6 July 2020; accepted 31 July 2020; published 13 August 2020)

Microwave absorption of a two-dimensional electron system (2DES) with a disk-shaped metallic gate has been investigated. We have found that relativistic plasmons are excited in the system when the gate is electrically connected to the 2DES. As a result, the 2DES is no longer electrically neutral during the plasma oscillation. This property significantly distinguishes “charged” relativistic plasmons from all other types of quasineutral plasma excitations. We have shown that the anomalously weak damping of relativistic plasmons is attributed to the hybridization of the plasmon with the photon mode of the external circuit. We have developed a theoretical basis for the relativistic plasmon phenomenon. The experimental data provide conclusive evidence in support of the theory.

DOI: [10.1103/PhysRevB.102.081301](https://doi.org/10.1103/PhysRevB.102.081301)

Plasma oscillations in two-dimensional electron systems (2DES) have been a subject of active research for over 50 years [1–11]. It has been established [1] that the spectrum of two-dimensional (2D) plasmons in the long-wavelength limit is given by

$$\omega_p(q) = \sqrt{\frac{n_s e^2 q}{2m^* \epsilon_0 \epsilon(q)}} \quad (q \gg \omega/c). \quad (1)$$

Here, q is the wave vector of the plasmon, while n_s and m^* are the density and effective mass of the 2D electrons. The effective permittivity for vacuum and surrounding medium are denoted by ϵ_0 and $\epsilon(q)$, respectively. Compared to plasmons in metals, one of the most prominent properties of 2D plasmons is their tunability over a wide frequency range achieved by changes in electron density.

However, the extensive application of 2D plasmonics is restricted considerably by the excitation condition $\omega_p \tau \gg 1$, where τ is the relaxation time of electrons. Thus, observation of 2D plasma waves is possible only at cryogenic temperatures in the terahertz frequency range, while in the infrared spectrum, it is limited to submicron propagation lengths [12]. Recently, it has been discovered that partly gated 2DES supports completely new kinds of plasma waves—relativistic [13,14] and proximity [15–18] plasmons. Relativistic plasmons were shown to possess several compelling physical properties. Most importantly, they exhibit anomalously weak damping. It is this property that makes it possible to observe relativistic plasmons at room temperature, with $\omega_p \tau \ll 1$, when ordinary 2D plasmons are overdamped. Although the phenomenology of the relativistic plasma waves has been ascertained, their physical origin remained a mystery for a long time.

The first step in shedding light on the essence of the relativistic plasmon was the discovery of proximity plasma

excitations [15–18]. These 2D plasma waves are observed when a highly conductive gate is placed in proximity to the 2DES. Their wave vector is directed along the gate strip with no potential nodes present in the transverse direction. It was found that the spectrum of the proximity plasmon combines unique features of gated plasmons with $\omega_g \propto \sqrt{h}$ [19], where h is the distance between the gate and the 2DES, and ungated plasma excitations with $\omega_p \propto \sqrt{q}$ [1].

In the present Rapid Communication, we unveil the physical nature of relativistic plasmons. By experiment, we discovered that a relativistic plasmon is not excited unless the gate is electrically connected to the 2DES via Ohmic contact. This means that the 2D electron subsystem does not remain electrically neutral during such plasma oscillation. Hence, the charge fluctuation in the 2DES is compensated by the charge of the opposite sign entering the gate through an external circuit. This particular feature sets the “charged” relativistic plasmon apart as a fundamentally new type of plasma excitation. Most importantly, we demonstrate that anomalously weak damping of relativistic plasma excitations is caused by strong interaction between the 2D plasma and the photon mode of the external circuit. Based on the proposed concept, we developed a theory that proved to be in good agreement with experimental data.

The experiments were conducted on $\text{Al}_{0.24}\text{Ga}_{0.76}\text{As}/\text{GaAs}/\text{Al}_{0.24}\text{Ga}_{0.76}\text{As}$ a single 30-nm-wide quantum well grown by molecular beam epitaxy. Under illumination, low-temperature electron density, n_s and mobility μ were $2.5 \times 10^{11} \text{ cm}^{-2}$ and $5 \times 10^6 \text{ cm}^2/\text{Vs}$, respectively. The quantum well was located at a distance of $h = 3700 \text{ \AA}$ below the crystal surface. The samples were patterned using optical lithography tools. The two-dimensional electron system had a form of a disk with a diameter of $D = 0.5 \text{ mm}$ (see the inset to Fig. 1 for a schematic drawing). Ohmic Au/Ge contact was made around the perimeter of the 2DES. Metallic gate of diameter

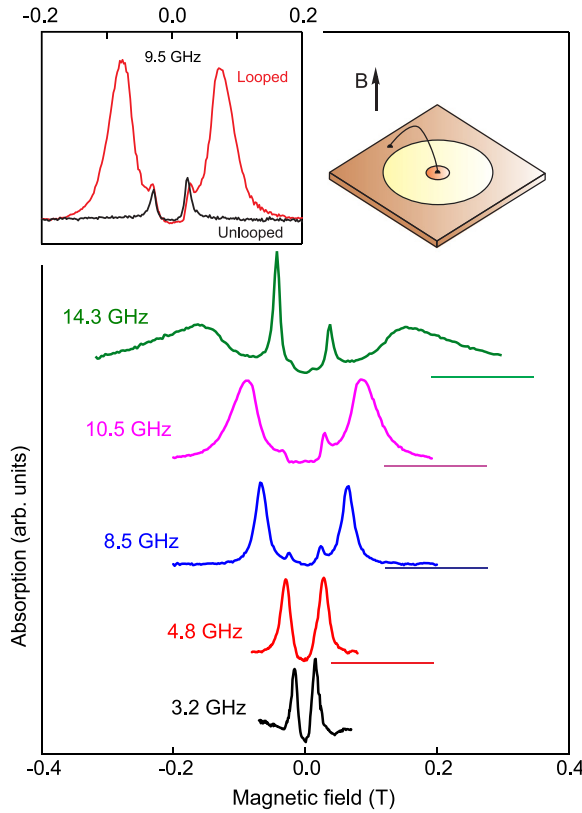


FIG. 1. Microwave absorption as a function of B , measured at $f = 3.2, 4.8, 8.5, 10.5,$ and 14.8 GHz for the sample with gate diameter $d = 100 \mu\text{m}$, 2D electron density $n_s = 2.5 \times 10^{11} \text{cm}^{-2}$, and wire loop length $l = 2.3$ mm. The curves are normalized and offset for clarity. Short horizontal lines indicate signal levels with no microwave excitation. The upper left inset displays absorption with and without the wire connecting the gate and the contact, plotted with the red and black curve, respectively. The upper right inset shows the sample setup.

d was thermally evaporated in the center of the 2DES. The gate diameter was varied between different samples fabricated from the same wafer, with $d = 100, 50, 40,$ and $20 \mu\text{m}$. The outer contact and inner gate were contacted by a wire of $25 \mu\text{m}$ in diameter and with a length of l . The radiation was guided into the cryostat with a coaxial cable and transferred to the sample via a transmission line ending with a whip antenna. Microwave radiation with frequencies from 0.01 to 50 GHz was used for the measurements. In order to detect the microwave absorption, we employed an optical technique [20,21]. For each experimental point, luminescence spectra were recorded consecutively, with and without microwave excitation. Then, the differential luminescence spectrum was calculated by subtracting the latter set of spectral data from the former one. The same procedure was repeated 3–10 times to enable averaging for improving the signal-to-noise ratio. Finally, the absolute value of the averaged differential spectrum was integrated over the entire spectral range to yield an estimate of microwave absorption. The sample was placed in a helium cryostat at the center of a superconducting solenoid. The sample temperature during measurements was $T = 1.5$ K.

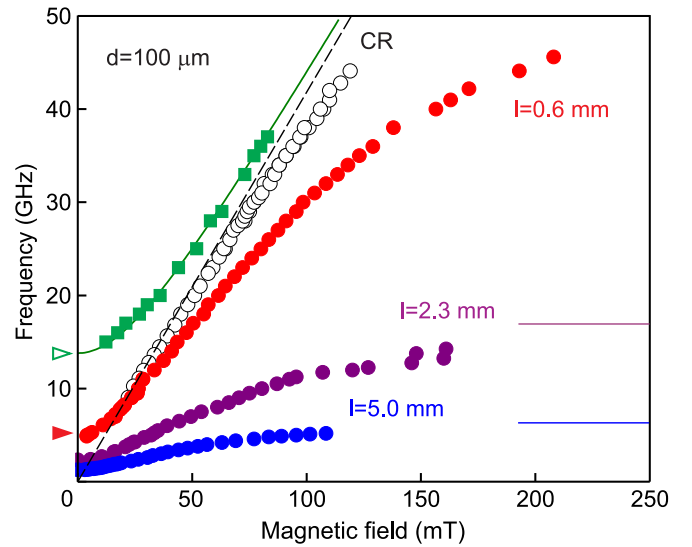


FIG. 2. Magnetic field dependence of plasma modes excited in the sample with fixed gate diameter $d = 100 \mu\text{m}$ and 2DES density $n_s = 2.5 \cdot 10^{11} \text{cm}^{-2}$, but different wire lengths $l = 0.6, 2.3$ and 5.0 mm. The plasma modes plotted in solid red, purple, and blue circles correspond to the relativistic plasmons for the specified wire loop lengths. Green squares designate magnetodispersion of the proximitry plasmon (1,0), empty black circles denote the single-particle (CR) resonance, and the dashed line represents the cyclotron frequency. Horizontal lines indicate the asymptotic frequencies f_i .

Figure 1 shows microwave absorption traces as a function of the applied magnetic field, recorded at excitation frequencies of 3.2, 4.8, 8.5, 10.5, and 14.3 GHz. The measurements were taken using the sample with the center-gate diameter $d = 100 \mu\text{m}$, and the bonding wire loop length $l = 2.3$ mm (see inset to Fig. 1). In the figure, the traces are offset vertically for clarity. According to plotted data, each trace contains up to three resonant peaks. The most prominent resonance occurs at 3.2 GHz. With increasing excitation frequency, this peak shifts rapidly in the direction of a stronger magnetic field. Finally, the peak broadens and disappears at a frequency of about 15 GHz. Such behavior is characteristic of plasmon hybridization with the photonic mode of the external resonator at frequency f_i [22–25]. In the discussion that follows, we corroborate that the observed plasma mode corresponds to the relativistic plasmon excitation [13,14]. Most importantly, the resonance disappears when the gate-contact loop is removed (see inset in Fig. 1). This finding suggests that the relativistic plasma wave has a very nontrivial current distribution. As the oscillating charge is transferred between the 2DES and the gate through the external circuit, 2D plasma is coupled to the electromagnetic field of the wire. In the case of strong retardation, the plasmon field is delocalized from the 2DES to the external circuit, acting as a photonic resonator. This leads to a phenomenally weak damping of relativistic plasma excitations.

To further substantiate this idea, we include in Fig. 2 magnetodispersion plots of all magnetoplasma modes measured on the same structure but with different lengths l of the wire loop which connects the central gate and the perimeteric contact. For each sample configuration, we observed

simultaneously three plasma modes (see Supplemental Material I for additional experimental data [26]). The relativistic plasma mode is indicated by colored dots. Most remarkably, both other modes are not affected by the presence of the wire loop. One of them closely follows the cyclotron resonance (CR) $\omega_c = eB/m^*$, as displayed with the empty circles in Fig. 2. The physical origin of this resonance is still not clear [31,32]. The third resonance (filled squares in Fig. 2) corresponds to excitation of the proximity plasmon localized near the gate [15–18]. This is confirmed by the observed magnetic-field dependence $\omega^2 = \omega_{\text{pr}}^2 + \omega_c^2$ (green curve in Fig. 2), and plasmon frequency at $B = 0$ T [33]:

$$\omega_{\text{pr}} = \Omega_{(m,n)} \sqrt{\frac{n_s e^2 \hbar}{m^* \varepsilon \varepsilon_0} \frac{2}{d}}. \quad (2)$$

Here, $\varepsilon = \varepsilon_{\text{GaAs}} = 12.8$, whereas the dimensionless frequency $\Omega_{(m,n)}$ is determined by the azimuthal m and radial n indices, referring to the number of plasma wave nodes along the 2DES disk circumference and radius, respectively. Considering that for the fundamental proximity plasmon mode, with $m = 1$ and $n = 0$, $\Omega_{(1,0)} = 2.4$, for the sample under study, Eq. (2) yields $f_{\text{pr}} = 14$ GHz, which is in good agreement with experimental results (empty arrow in Fig. 2).

For a quantitative frequency estimate of the relativistic plasma mode, we treated plasma excitations in the 2DES as an equivalent LC plasmonic resonator [16,27,28]. In this approach, L corresponds to the 2DES kinetic inductance of non-magnetic origin, while C represents the electrical capacitance between 2DES and the gate. Thus, provided that the charged capacitor is electrically connected to the 2DES inductor, the circuit undergoes LC oscillations. The LC plasma oscillations should belong to the proximity plasmon family with $m = 0$ and $n = 0$. Consequently, assuming the net impedance of the wire loop to be zero, the theoretical analysis yields the dispersion equation for the relativistic plasmons $J_0(\Omega) - \Omega J_1(\Omega) \ln(D/d) = 0$, where J_0 and J_1 are Bessel functions of the first kind, and $\Omega = \omega d / [2\sqrt{n_s e^2 \hbar / (m^* \varepsilon \varepsilon_0)}]$ is the dimensionless plasmon frequency (for details, see Supplemental Material II [26]). Then, using Bessel function expansions, the relativistic plasmon frequency can be expressed explicitly as

$$\omega_{\text{rel}} = \sqrt{\frac{2}{1/4 + \ln(D/d)}} \sqrt{\frac{n_s e^2 \hbar}{m^* \varepsilon \varepsilon_0} \frac{2}{d}} \quad (D/d > 2). \quad (3)$$

Indeed, according to the magnetodispersion curve for the sample with $l = 0.6$ mm (Fig. 2), at $B = 0$ T, the relativistic plasma frequency $f_{\text{rel}} = 5$ GHz, which agrees reasonably well with the calculated value of 6 GHz (solid arrow in Fig. 2) predicted by Eq. (3). It should be noted that our theoretical results are compared with experimental data for the sample with the smallest practically achievable length of wire loop $l = 0.6$ mm. In this case, we maximally reduce the retardation effects, unaccounted for by our approximation hypothesis. To provide further experimental support for the theory, we conducted additional experiments on the samples fabricated from the same wafer, with fixed 2DES diameter $D = 0.5$ mm, and different gate diameters $d = 50, 40, 20$, and 10 μm . Figure 3(a) shows the resultant frequencies of the relativistic (0,0) and proximity (1,0) plasmons plotted versus the

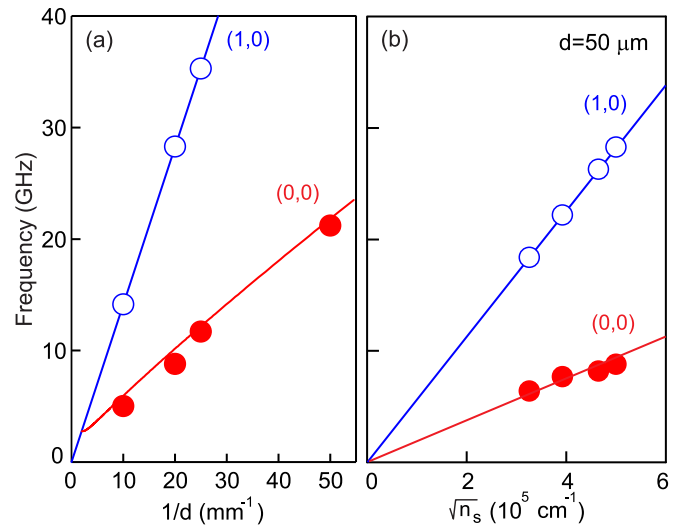


FIG. 3. (a) Dependence of the plasmon frequency on the reciprocal of the gate diameter, $1/d$, for the sample with 2D electron density $n_s = 2.5 \times 10^{11} \text{ cm}^{-2}$, 2DES diameter $D = 0.5$ mm, and wire loop length $l = 0.6$ mm. (b) Dependence of the plasmon frequency on the square root of 2D electron density, for the sample with gate diameter $d = 50 \mu\text{m}$ and 2DES diameter $D = 0.5$ mm. Red and blue lines denote theoretical predictions for the relativistic (0,0) and proximity (1,0) plasmons, respectively.

reciprocal of the gate diameter, $1/d$. Theoretical predictions according to Eq. (3) (red curve) and Eq. (2) (blue curve) are in good agreement with experimental data. Here, we note that the observed (0,0) mode frequencies consistently appear to be slightly below the theoretical values, presumably due to the parasitic inductance of the wire loop.

One of the most outstanding properties of two-dimensional electron systems is their tunability. In our experiments, we changed the 2D electron density in the given structure using a photodepletion method [34]. Figure 3(b) shows that when the electron density was tuned from $n_s = 2.5 \times 10^{11} \text{ cm}^{-2}$ to $1.0 \times 10^{11} \text{ cm}^{-2}$, the plasmon frequency of both proximity (1,0) and relativistic (0,0) modes demonstrate a corresponding decrease. The experiment was conducted on the structure with dimensions $d = 50 \mu\text{m}$ and $D = 0.5$ mm and the smallest attainable length of the wire $l = 0.6$ mm. Lines in Fig. 3(b) show square-root dependencies $\sqrt{n_s}$ according to Eqs. (2) and (3).

One of the most compelling features of the relativistic plasma wave is its anomalously small damping. Relativistic plasmons survive in high-conductivity structures even at temperatures up to 300 K, opening an avenue for many applications [14]. The data in Fig. 2 suggest that this feature is associated with the strong interaction of the plasma wave with the photon mode of the external circuit—the wire loop. Physically, such a considerable reduction in plasmon damping originates from the delocalization of the plasmon mode into the photon resonator [25]. Indeed, for the sample with wire length $l = 5$ mm, the magnetodispersion of the relativistic plasmon (blue circles in Fig. 2) crosses the CR line, demonstrating substantial retardation. After that it asymptotically reaches a photon plateau at $f_l = 6.6$ GHz. Such a behavior is

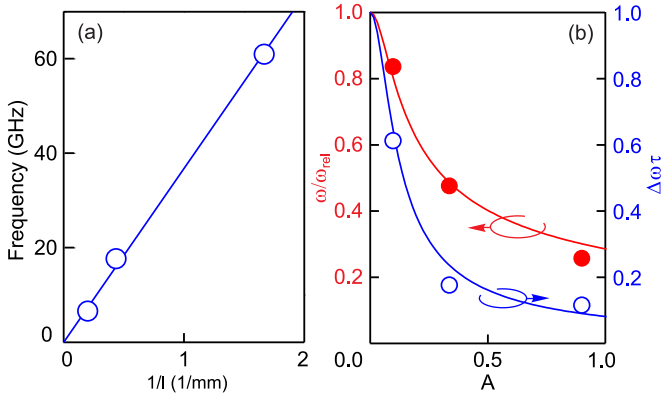


FIG. 4. (a) Photon frequency f_i versus the reciprocal wire length. (b) Normalized relativistic plasmon frequency $\omega/\omega_{\text{rel}}$ (solid red circles) and half-width $\Delta\omega\tau$ (empty blue circles) as a function of retardation parameter $A = \omega_{\text{rel}}/2\pi f_i$. Red and blue curves denote the prediction for an ordinary 2D plasmon, based on Equations (4).

typical for plasmon-polariton excitations [22–25]. As shown in Fig. 4(a), photon frequencies measured for the samples with $l = 0.6, 2.3,$ and 5 mm scale linearly with $1/l$, which confirms that the wire acts as a resonator, coupling to 2D plasma oscillations. It is also worth mentioning that experimental values of f_i are in good agreement with the resonant frequency of a straight wire placed directly above the GaAs crystal, $f_l = c/\sqrt{4l\epsilon^*}$ (see Supplemental Material III [26]).

Hybridization of the 2D plasma and light modes usually leads to a significant decrease in the plasma resonant frequency along with suppression of the plasmon damping [22–25]. Analogous effects are observed in the case of relativistic plasma excitation. Indeed, Fig. 4(b) illustrates how normalized relativistic plasmon frequency $\omega/\omega_{\text{rel}}$ (solid red circles) and half-width $\Delta\omega\tau$ (empty blue circles) depend on a retardation parameter A . The retardation parameter A was defined as the ratio of ω_{rel} to the frequency of light $2\pi f_l$. The resultant dependencies are qualitatively similar to those obtained for ordinary 2D plasmon-polariton modes excited in a disk [22,25]. However, the magnitude of the observed effect far exceeds the level expected for the ordinary 2D plasmons. According to the 2D-plasmon theory [22,23],

$$\omega^2 = \frac{\omega_p^2}{\sqrt{1+A^2}}, \quad \Delta\omega = \frac{1}{\tau} \frac{1}{\sqrt{1+A^2}}. \quad (4)$$

However, our experiments reveal that plasmon-photon coupling of the relativistic plasmons is a great deal stronger than that of the ordinary 2D plasmons. For this reason, measurement data and theoretical curves [red and blue lines in Fig. 4(b)] predicted by Equations (4) show close agreement only when retardation parameter $A_{\text{rel}} = 12A$.

Generally, the interaction of matter with light is quantified by the Rabi frequency Ω_{Rabi} . Figure 5(a) shows the relativistic plasmon frequency at $B = 0$ T plotted versus the wave vector of the wire photon mode $q = \pi/2l$. Here, we used experimental data for the sample with $D = 0.5$ mm and $d = 100$ μm displayed in Fig. 2. The dispersion of light and relativistic plasmon is denoted, respectively, by the solid red and dashed blue lines, whereas the solid blue line

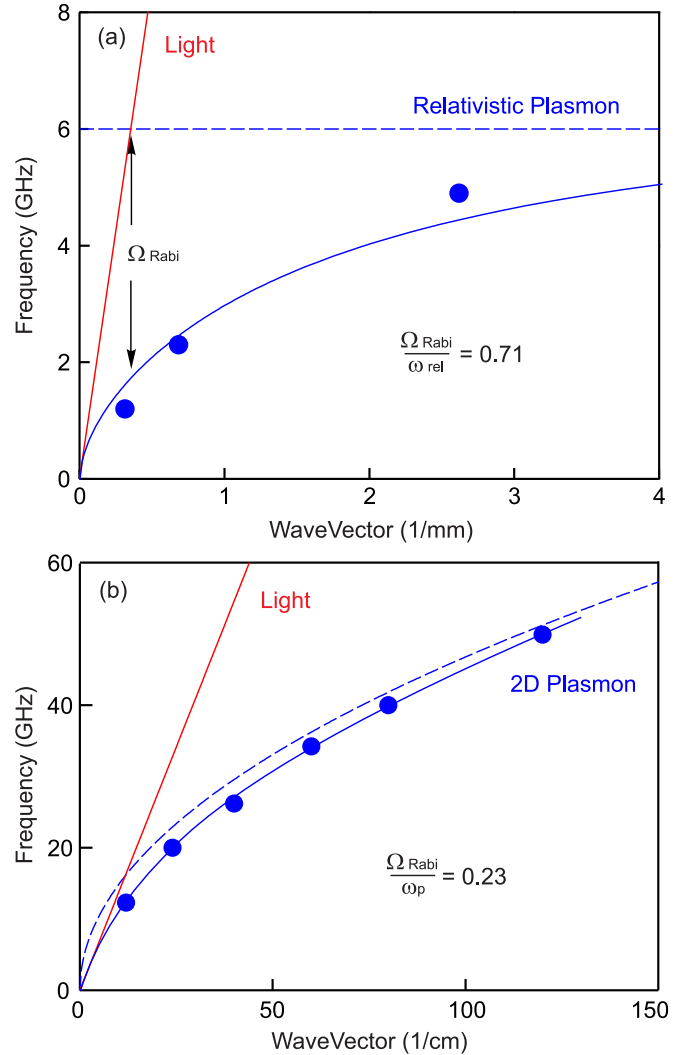


FIG. 5. (a) Dispersion of the relativistic plasmon-polariton excitation for the sample with $D = 0.5$ mm and $d = 100$ μm . (b) Dispersion of the ordinary 2D plasmon-polariton measured on a set of disk-shaped 2DES, fabricated from the same wafer. Solid red and dashed blue lines designate the dispersion of light and the plasmon dispersion calculated in the quasistatic approximation. Solid blue curves display dispersion according to Eq. (4).

designates the dispersion based on Eq. (4), with $A_{\text{rel}} = 12A$. There is clear evidence for ultrastrong coupling between the relativistic plasmon and the electromagnetic mode in a wire with $\Omega_{\text{Rabi}}/\omega_{\text{rel}} = 0.71$. For the sake of comparison, we also measured the dispersion of 2D plasmon polaritons in a set of bare disk-shaped 2DESs with no gates or contacts present. The samples were fabricated from the same wafer, with $n_s = 2.5 \times 10^{11}$ cm^{-2} , having a disk-shaped mesa of different diameter $a = 2, 1, 0.6, 0.4, 0.3,$ and 0.2 mm. In Fig. 5(b), we include the resonance frequency data plotted as a function of the inverse of the mesa diameter $q = 2.4/a$ [22]. There is a hybridization of the 2D plasma and light modes. However, found normalized Rabi frequency $\Omega_{\text{Rabi}}/\omega_p = 0.23$ is much less than that for the relativistic plasmon.

In conclusion, we have investigated relativistic plasma excitation in a high-mobility AlGaAs/GaAs 2DES with disk

geometry. We have found the electrical connection between the gate and 2DES to be crucial for the excitation of the relativistic plasmon. We also recognized that at the time of plasma oscillation, the two-dimensional system loses its electrical neutrality. This property uniquely distinguishes “charged” relativistic plasmons among all other types of quasineutral plasma waves. Importantly, we developed a theory to expound on the physical origin of relativistic plasmons. As a result, we established that their exceptionally

weak damping is related to the ultrastrong hybridization of 2D plasma with light, which is particularly promising for developing microwave and terahertz sensing and generation devices.

The authors gratefully acknowledge financial support from the Russian Foundation for Basic Research (Grant No. 18-02-00753 for experiment, Grant No. 20-32-70188 for theory, and Grant No. 20-02-00817 for numerical simulations).

-
- [1] F. Stern, *Phys. Rev. Lett.* **18**, 546 (1967).
- [2] C. C. Grimes and G. Adams, *Phys. Rev. Lett.* **36**, 145 (1976).
- [3] S. J. Allen, Jr., D. C. Tsui, and R. A. Logan, *Phys. Rev. Lett.* **38**, 980 (1977).
- [4] T. N. Theis, J. P. Kotthaus, and P. J. Stiles, *Solid State Commun.* **24**, 273 (1977).
- [5] U. Mackens, D. Heitmann, L. Prager, J. P. Kotthaus, and W. Beinvogl, *Phys. Rev. Lett.* **53**, 1485 (1984).
- [6] D. C. Glatli, E. Y. Andrei, G. Deville, J. Poitrenaud, and F. I. B. Williams, *Phys. Rev. Lett.* **54**, 1710 (1985).
- [7] T. Demel, D. Heitmann, P. Grambow, and K. Ploog, *Phys. Rev. Lett.* **66**, 2657 (1991).
- [8] G. Scalari, C. Maissen, D. Turcinkova, D. Hagenmüller, S. De Liberato, C. Ciuti, C. Reichl, D. Schuh, W. Wegscheider, M. Beck, and J. Faist, *Science* **335**, 1323 (2012).
- [9] G. C. Dyer, G. R. Aizin, S. James Allen, A. D. Grine, D. Bethke, J. L. Reno, and E. A. Shaner, *Nat. Photonics* **7**, 925 (2013).
- [10] D. A. Iranzo, S. Nanot, E. J. C. Dias, I. Epstein, C. Peng, D. K. Efetov, M. B. Lundberg, R. Parret, J. Osmond, Jin-Yong Hong, J. Kong, D. R. Englund, N. M. R. Peres, and F. H. L. Koppens, *Science* **360**, 291 (2018).
- [11] D. A. Bandurin, D. Svinsov, I. Gayduchenko, S. G. Xu, A. Principi, M. Moskotin, I. Tretyakov, D. Yagodkin, S. Zhukov, T. Taniguchi, K. Watanabe, I. V. Grigorieva, M. Polini, G. N. Goltsman, A. K. Geim, and G. Fedorov, *Nat. Commun.* **9**, 5392 (2018).
- [12] G. X. Ni, A. S. McLeod, Z. Sun, L. Wang, L. Xiong, K. W. Post, S. S. Sunku, B. Y. Jiang, J. Hone, C. R. Dean, M. M. Fogler, and D. N. Basov, *Nature (London)* **557**, 530 (2018).
- [13] P. A. Gusikhin, V. M. Muravev, and I. V. Kukushkin, *JETP Lett.* **100**, 648 (2015).
- [14] V. M. Muravev, P. A. Gusikhin, I. V. Andreev, and I. V. Kukushkin, *Phys. Rev. Lett.* **114**, 106805 (2015).
- [15] A. A. Zabolotnykh and V. A. Volkov, *Phys. Rev. B* **99**, 165304 (2019).
- [16] V. M. Muravev, P. A. Gusikhin, A. M. Zarezin, I. V. Andreev, S. I. Gubarev, and I. V. Kukushkin, *Phys. Rev. B* **99**, 241406(R) (2019).
- [17] V. M. Muravev, A. M. Zarezin, P. A. Gusikhin, A. V. Shupletsov, and I. V. Kukushkin, *Phys. Rev. B* **100**, 205405 (2019).
- [18] A. M. Zarezin, P. A. Gusikhin, V. M. Muravev, and I. V. Kukushkin, *JETP Lett.* **111**, 282 (2020).
- [19] A. V. Chaplik, *Zh. Eksp. Teor. Fiz.* **62**, 746 (1972) [*Sov. Phys. JETP* **35**, 395 (1972)].
- [20] B. M. Ashkinadze, E. Linder, and V. Umansky, *Phys. Rev. B* **62**, 10310 (2000).
- [21] I. V. Kukushkin, J. H. Smet, K. von Klitzing, and W. Wegscheider, *Nature (London)* **415**, 409 (2002).
- [22] I. V. Kukushkin, J. H. Smet, S. A. Mikhailov, D. V. Kulakovskii, K. von Klitzing, and W. Wegscheider, *Phys. Rev. Lett.* **90**, 156801 (2003).
- [23] S. A. Mikhailov and N. A. Savostianova, *Phys. Rev. B* **71**, 035320 (2005).
- [24] V. M. Muravev, I. V. Andreev, I. V. Kukushkin, S. Schmult, and W. Dietsche, *Phys. Rev. B* **83**, 075309 (2011).
- [25] P. A. Gusikhin, V. M. Muravev, A. A. Zagitova, and I. V. Kukushkin, *Phys. Rev. Lett.* **121**, 176804 (2018).
- [26] See Supplemental Material at <http://link.aps.org/supplemental/10.1103/PhysRevB.102.081301>, which includes Refs. [27–30], for additional experimental data, theoretical treatment of the relativistic plasma excitation, and evaluation of the frequency of wire resonator.
- [27] P. J. Burke, I. B. Spielman, J. P. Eisenstein, L. N. Pfeiffer, and K. W. West, *Appl. Phys. Lett.* **76**, 745 (2000).
- [28] G. R. Aizin and G. C. Dyer, *Phys. Rev. B* **86**, 235316 (2012).
- [29] V. A. Volkov and S. A. Mikhailov, *JETP Lett.* **42**, 556 (1985).
- [30] A. L. Fetter, *Phys. Rev. B* **32**, 7676 (1985).
- [31] S. I. Dorozhkin, A. A. Kapustin, I. A. Dmitriev, V. Umansky, K. von Klitzing, and J. H. Smet, *Phys. Rev. B* **96**, 155306 (2017).
- [32] I. V. Andreev, V. M. Muravev, V. N. Belyanin, and I. V. Kukushkin, *Phys. Rev. B* **96**, 161405(R) (2017).
- [33] A. A. Zabolotnykh and V. A. Volkov, *Semiconductors* **53**, 1870 (2019).
- [34] I. V. Kukushkin, K. von Klitzing, K. Ploog, V. E. Kirpichev, and B. N. Shepel, *Phys. Rev. B* **40**, 4179 (1989).